NRIAG Journal of Astronomy and Geophysics (2013) 2, 250–255

National Research Institute of Astronomy and Geophysics

NRIAG Journal of Astronomy and Geophysics

www.elsevier.com/locate/nrjag

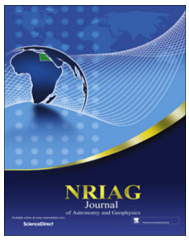

Automatic concrete cracks detection and mapping of terrestrial laser scan data

Mostafa Rabah [a,*], Ahmed Elhattab [b], Atef Fayad [c]

[a] *National Research Institute of Astronomy and Geophysics, Helwan Cairo, Egypt*
[b] *Port Said University, Faculty of Engineering, Egypt*
[c] *Ain Shams University, Faculty of Engineering, Egypt*

Received 7 June 2013; revised 5 December 2013; accepted 8 December 2013
Available online 31 December 2013

KEYWORDS

Crack detection and mapping;
Terrestrial laser scan;
Median filter;
Probabilistic relaxation

Abstract Terrestrial laser scanning has become one of the standard technologies for object acquisition in surveying engineering. The high spatial resolution of imaging and the excellent capability of measuring the 3D space by laser scanning bear a great potential if combined for both data acquisition and data compilation. Automatic crack detection from concrete surface images is very effective for nondestructive testing. The crack information can be used to decide the appropriate rehabilitation method to fix the cracked structures and prevent any catastrophic failure. In practice, cracks on concrete surfaces are traced manually for diagnosis. On the other hand, automatic crack detection is highly desirable for efficient and objective crack assessment.

The current paper submits a method for automatic concrete cracks detection and mapping from the data that was obtained during laser scanning survey. The method of cracks detection and mapping is achieved by three steps, namely the step of shading correction in the original image, step of crack detection and finally step of crack mapping and processing steps. The detected crack is defined in a pixel coordinate system. To remap the crack into the referred coordinate system, a reverse engineering is used. This is achieved by a hybrid concept of terrestrial laser-scanner point clouds and the corresponding camera image, i.e. a conversion from the pixel coordinate system to the terrestrial laser-scanner or global coordinate system. The results of the experiment show that the mean differences between terrestrial laser scan and the total station are about 30.5, 16.4 and 14.3 mms in x, y and z direction, respectively.

1. Introduction

According to (Laefer et al., 2010) the Spatial referencing of damage is encouraged through measuring and counting repetitive materials, such as bricks and windows. A more engineering-oriented approach was proposed by American Society of Civil Engineers (ASCE, 2000a,b), focusing on structural aspects based on material composition. An incremental, multilevel

* Corresponding author. Tel.: +20 1000487605.
E-mail addresses: mostafa_rabah@yahoo.com, mostafa.rabah@gmail.com (M. Rabah).

Peer review under responsibility of National Research Institute of Astronomy and Geophysics.

ELSEVIER Production and hosting by Elsevier

2090-9977 © 2013 Production and hosting by Elsevier B.V. on behalf of National Research Institute of Astronomy and Geophysics.
http://dx.doi.org/10.1016/j.nrjag.2013.12.002

intervention methodology was advised, due to the high cost of comprehensive assessments. As part of that process, both destructive and non-destructive testing for determining physical conditions and visual examinations were proposed for concrete and masonry structures. Visual examination (with or without optical aids), along with the measurement of tools and photographic records was suggested for evaluating surface condition deficiencies in joints and determining differential movement. Surveying tools and instruments were recommended to aid in the recording of crack size, alignment, and location. Visual examination was found to detect the widest range of physical degradation in both concrete and masonry, even more so than more active forms of non-destructive testing.

The Terrestrial Laser-Scanner (TLS) generates 3D-coordinates of an object point by measuring the horizontal and vertical angle and the distance between the scanner's center and the object point. This happens with high performance. Depending on the type of scanner and the method of distance measurement used (time of flight or phase difference), it produces from 1000 points per second (Cyrax 2500) up to over 900,000 points per second (Faro Photon) (Van Gosliga et al., 2006). The density of points on the object's surface can be predefined by the user and is limited by the minimum angle increment of the system. Depending on the distance from the scanner and the amount of scans, a very high point density can be achieved. But high point density does not coincide with high accuracy. The accuracy of a single point depends primarily on the accuracy of the distance measurement. Depending on different types of scanners and different methods, achievable accuracies of distance measurement vary from sub-millimeters to some centimeters.

In addition, the reflectance of the surface may be measured by recording the intensity of the reflected laser beam, although this way of generating a gray-level image is limited to the wavelength of the laser beam. A more sophisticated technique is able to measure true color intensities at each laser dot location in a separate measurement step practically simultaneously to the distance registration (Van Gosliga et al., 2006). There is a certain drawback that has to be taken into consideration: the spatial resolution of laser measurements is limiting the practically possible resolution of conventional imaging. Therefore, current laser scanners use a combination of the two sensors – the distance measurement unit and a separate digital camera unit. The camera captures the full surrounding view in one scan. It operates by rotating around the vertical axis. A linear array CCD sensor captures the scenery as a continuous set of vertical scan lines. The advantages of this technology with respect to the others are:

- Digital cameras could provide a higher spatial resolution than laser scanners.
- The relative geometrical stability (from one point to the other) is guaranteed by the CCD sensor matrix, while the laser beam is individually positioned between each measurement, representing a dynamic principle.
- High information content, since a single image contains a full 360° scan.

By measuring a few reference points for each scan, the object can be transformed into a geo-referenced co-ordinate system, which enables the user to locate any part of an object in real 3D space. Therefore, 3D measurement and documentation of an object can be more quickly recorded in a 3D visual and digital format. The largest problem so far has been to handle the data output. It is not very difficult to carry out a 3D laser scan survey, but it has been quite hard to convert the data to useful information that can directly be used in engineering practice. The current research applies a robust automatic crack detection method from noisy concrete surfaces as described by (Fujita and Hamamoto, 2010). Additionally, a method for mapping the detected crack is explained.

2. Method of automatic crack detection

With crack detection, it is desired to extract the geometrical structure and direction of a crack by emphasizing its pixel values and muting the remaining pixels 'i.e. noise'. The noise elements can be compromised of shadings, blebs, stains and/or non-uniform light distribution that occurred during the photographing procedure. In order to remove the various noise elements a number of filtering and image processing procedures are executed.

2.1. Shading correction

In the conventional method, a corrective image photographed in advance is needed to remove the shading effect by dividing the input image with the corrective image. In a more practical approach, no additional images are needed. Instead, the corrective image is generated via the input image by applying a median filter on the input image. The median filter is a non-linear digital filtering technique applied by a sliding-window spatial filter that replaces the center value of the window 'i.e. kernel' with the median of all pixel values in the window. The kernel structure is usually square but can also be of any shape. With this technique the corrective image is a smoothed version of the input image.

The next step generates the output image by subtracting the corrective image from the input image. Fig. 1 illustrates the removal process of the slight variation values from the input image. By the subtraction process the slight variation of the smoothed image is eliminated from the output image. The output image is obtained by (Fujita and Hamamoto, 2010):

$$I_S(x_i) = \max\begin{cases} \text{median}_{x_{j\in R_i}} I(x_j) - I(x_i) \\ 0 \end{cases} \quad (1)$$

where: $I(x)$ means the intensity of the pixel x, and R_i means the region around the pixel x_i.$I_S(x_i)$ means the intensity of the smoothed image.

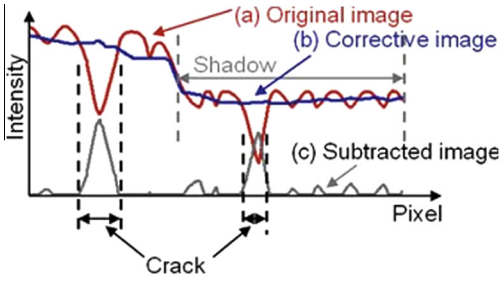

Fig. 1 Removal of serious variations like shading (Fujita and Hamamoto, 2010).

Fig. 2 depicts an example of an input image, the original, and the filter application of the shading correction, then the subtracting process to isolate the crack.

2.2. Detection processing

With manual crack detection, the human operator traces the crack manually on the input image. The crack is traced from its starting point until the termination point then labeled. To automate this step, the probabilistic relaxation technique is used to solve the labeling problem and to extract the crack trace from the noisy shading filtered image in step 1.

Probabilistic relaxation is mainly used as the optimization technique for solving labeling problem (Peleg, 1980; Henerson, 1990). By probabilistic relaxation, it is possible to label objects to be extracted from noisy data. However, the algorithm computes the probability by searching through the neighbor pixels, Fig. 2, in all directions, at 0° and at 45°.

The algorithm is structured from three steps:

1. Logarithmic scaling function to increase the difference between strong and low pixel intensity.
2. Probabilistic relaxation function that searches in four direction (d), and select the maximum probability value.
3. Weight function, in this case it is the average intensity of neighbor pixels.

To perform the automatization process by probabilistic relaxation, the following steps are executed:

First, an initial probability $P_i(\lambda_c)$ of the crack is assigned to logarithmic transformation of the output image of shading correction step through:

$$P_i(\lambda_c) = \frac{\log(R(x_i)+1)}{\log(R_{\max}+1)} \tag{2}$$

where $P_i(\lambda_c)$ is the initial probability of the crack. $R(x_i)$ means the output of the pre-processing at pixel x_i, $R_{\max}$ is the maximum value, and λ_c means the label for the crack.

Second, updating probabilities is done by considering the probabilities of neighboring pixels. The updating rule proposed by (Fujita and Hamamoto, 2010) is:

$$P'_i\lambda_c = \max \frac{P_i(\lambda_c)Q_i^d(\lambda_c)}{P_i(\lambda_c)Q_i^d(\lambda_c) + P_i(\lambda_b)Q_i^d(\lambda_b)} \tag{3}$$

$$Q_i^d(\lambda_k) = \frac{1}{N(R_i^d)} \sum_{x_l \in R_i^d} P_i(\lambda_l)$$

where $P_i(\lambda_b)$ is the probability of background where $P_i(\lambda_b) = 1 - P_i(\lambda_c)$, and λ_b is the label for background.

The technique divides the neighboring region into four subregions R_i^d along the angular direction $d = (0, 1/4\pi, 1/2\pi,$ and $3/4\pi)$ passing through the focal pixel. Therefore, $Q_i^d(\lambda_c)$ is

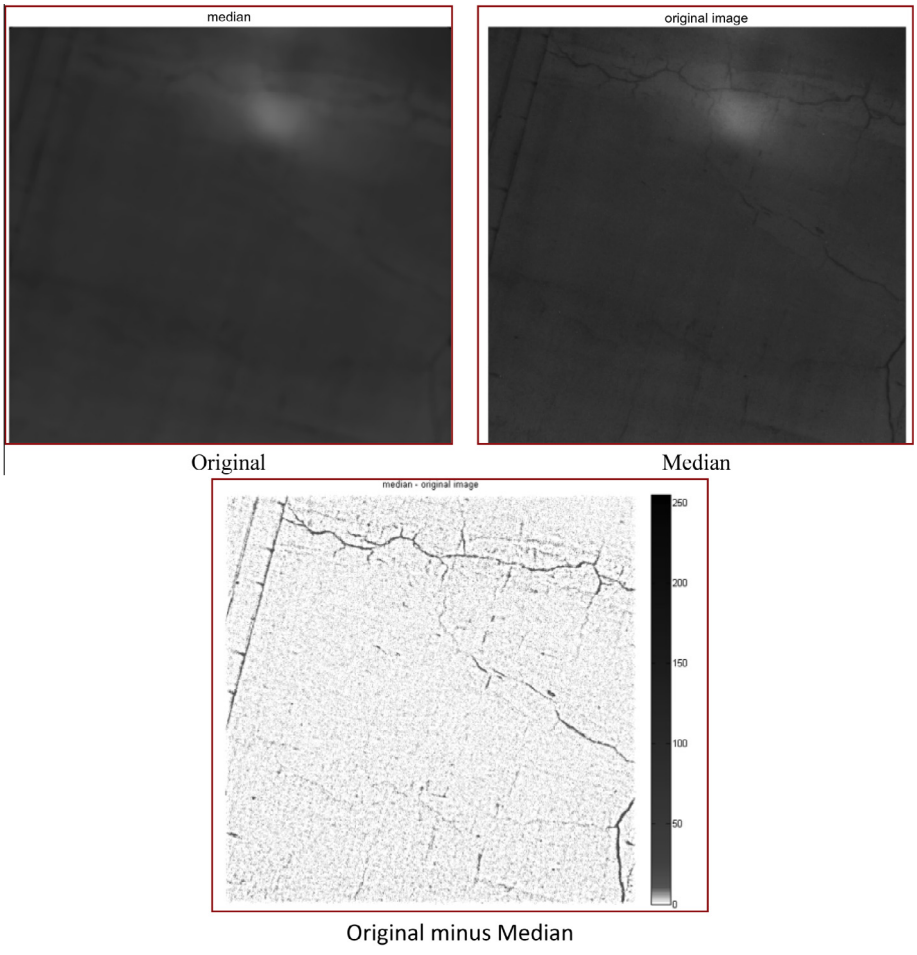

Fig. 2 A corrective image after applying the filter.

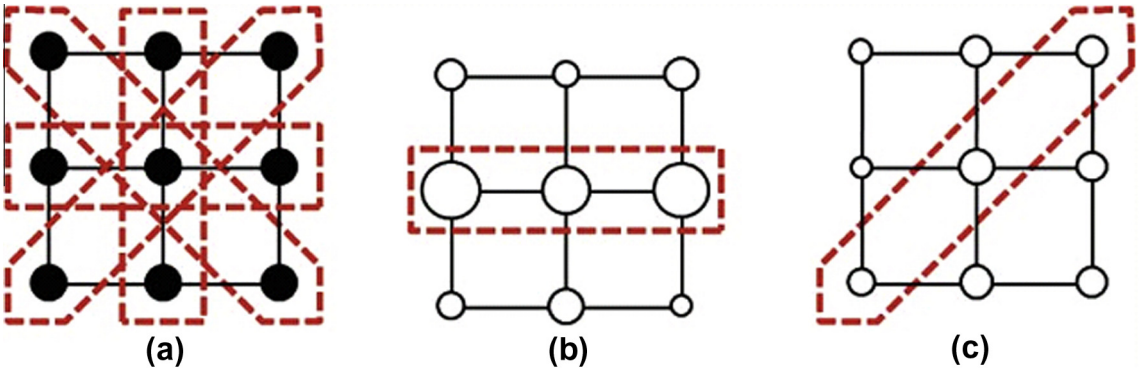

Fig. 3 Explanation of four sub-regions and updating in relaxation. (a) Division of four sub-regions. (b) Up case of an updating probability. (c) Down case of an updated probability, where each circle indicates a pixel and the central circle means the focal pixel. In (b) and (c), the selected sub-region in updating or the focal pixel is enclosed by a dot line (Fujita and Hamamoto, 2010).

regarded as the directional weighting function of support that the crack label λ_k at pixel x_i gets from its neighboring pixels. In this case, it is the directional average estimate for label λ_k in neighbors of x_i and $N(R_i^d)$ means the number of pixels in the sub- region R_i^d. By this process, noises in the image are expected to be removed by updating the process, whereas cracks remain, see Fig. 3.

3. Fracture mapping

After the crack detecting process, the pixels that define the crack geometry are, in general, defined in pixel coordinate systems where they are related by a set of physical parameters such as:

- The focal length of the lens.
- The size of the pixels.
- The position of the principal point.
- The position and orientation of the camera.

Two types of parameters need to be recovered in order to reconstruct the 3D structure of a scene from the pixel coordinates of its image points:

- Intrinsic camera parameters: the parameters necessary to link the pixel coordinates of an image point with the corresponding coordinates in the camera reference frame.
- Extrinsic camera parameters: the parameters that define the location and orientation of the camera reference frame with respect to a known world reference frame.

In order to remap the fractures from a local image coordinate to the real world coordinate, we use the inverse perspective transformation concept, demonstrated in Fig. 4. (Amiri Parian and Gruen, 2003) proposed a mapping function for the pinhole model-based perspective transformation in the form of bundle equations by assuming that the image space is ideally a pixel. It is assumed that the original image observations are saved in the pixel coordinate system as (i, j), see Fig. 5. Fig. 6 shows the other coordinate systems: linear array (0, y, z), auxiliary (X', Y', Z'), and object space (X, Y, Z) coordinate systems. The effects of lens distortion and the shift of the principle point are modeled in the linear array coordinate system. The rotation of the linear array and some systematic errors related to the rotation are modeled in the auxiliary coordinate system. The object space coordinate system is used as a reference for determining the exterior orientation parameters of the TLS.

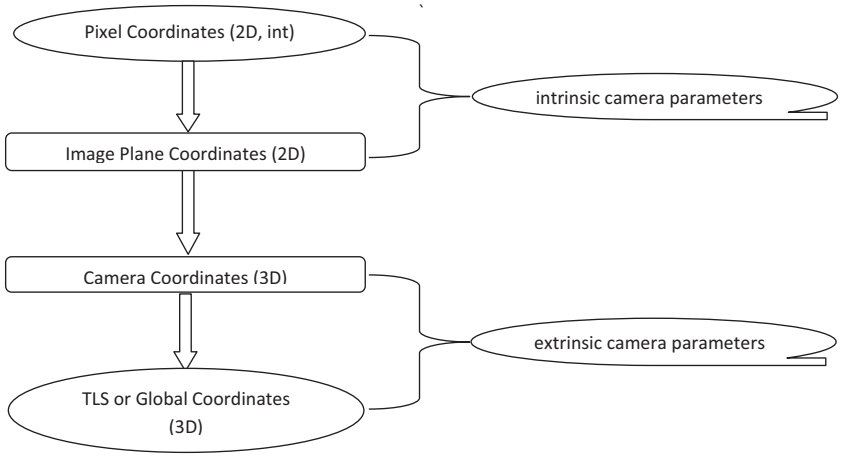

Fig. 4 A sketch represents the flow steps of the mapping process.

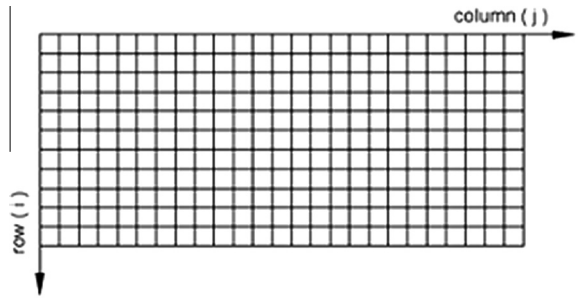

Fig. 5 Pixel coordinate system.

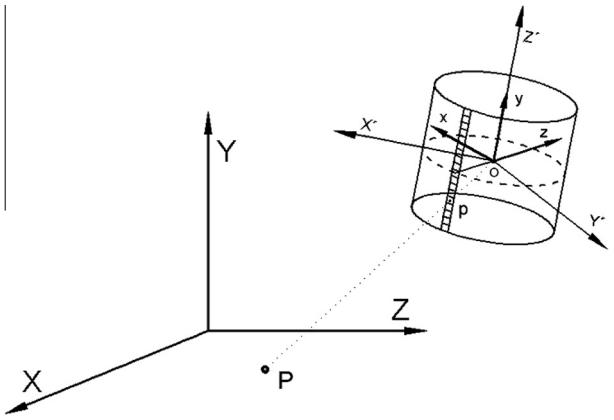

Fig. 6 Object coordinate (X, Y, Z), auxiliary coordinate (X', Y', Z') and Linear Array (0, y, z) coordinate systems.

The model, which relates image observations (i, j) to the object points (X, Y, Z), for an ideal sensor finally becomes:

$$\begin{pmatrix} 0 \\ y \\ -c \end{pmatrix} = \lambda P^{-1} R_Z^t(jA_h) M_{w,\varphi,k} \begin{pmatrix} X - X_0 \\ Y - Y_0 \\ Z - Z_0 \end{pmatrix} \quad (4)$$

with:

$$P = \begin{bmatrix} 0 & 0 & -1 \\ -1 & 0 & 0 \\ 0 & 1 & 0 \end{bmatrix} \text{ and } y = \left(i - \frac{N}{2}\right) A_V$$

where:

$\boldsymbol{M}_{w,\phi,k}$: 3 by 3 rotation matrix.
($\boldsymbol{X0}$, $\boldsymbol{Y0}$, $\boldsymbol{Z0}$): location of the origin of the auxiliary coordinate system in the object space coordinate system.
($\boldsymbol{X}$, $\boldsymbol{Y}$, $\boldsymbol{Z}$): coordinates of points in object space.
($\boldsymbol{X'}$, $\boldsymbol{Y'}$, $\boldsymbol{Z'}$): coordinates of object points in the auxiliary coordinate system.
$\boldsymbol{A_h}$: resolution of rotation.
$\boldsymbol{A_v}$: pixel size of the linear array.
C: camera constant.
$\boldsymbol{N}$: total number of rows or number of pixels in the linear array.
$\boldsymbol{R_z}$: 3D rotation matrix around $\boldsymbol{Z}$ axis.
$\boldsymbol{P}$: transfer matrix from the linear array to the auxiliary coordinate system.
($\boldsymbol{0}$, $\boldsymbol{y}$, $\boldsymbol{-c}$): coordinates of image points in the linear array coordinate system.
($\boldsymbol{i}$, $\boldsymbol{j}$): coordinates of image points in the pixel coordinate system.

4. Experimental results

To verify the aforementioned method, a survey scan with Leica C10 TLS for one of Macca tunnels in KSA was done. The used Leica C10 has the following characteristics (Leica ScanStation C10 brochure): it is based on a pulsed laser scanner operating at a wavelength of 532 nm. It is provided with an integrated color digital camera with zoom video. It is able to acquire a scene of single $17° \times 17°$ image: 1920×1920 pixels with a field of view of up to 360° horizontal und 270° vertical in a single scan, 230 images. The typical standoff distance is 75–150 m, but measurements of more than 300 m are possible. The accuracy of a single point measurement is specified with 3–6 mm. In the experiment we made an attempt of assessment of the accuracy of data acquisition and registration.

Fig. 2 shows a sample of the original image with gray color (the left view), the right view is updated image after applying the median filter. The third view is resulted from subtracting the right view from the original image. As it is shown in the third image, one can easily notice how the median filter based algorithm support the user in getting more sharpened view of the crack. Fig. 7 depicts the location of the detected crack in the World Coordinate System of the TLS after mapping it by the proposed method.

In evaluation, we compared the proposed approach with the conventional approach of the tracing the crack by utilizing a survey equipment. The Leica 1230 Total station was used manually to survey some marked points on the crack, occupying the same setup point of the TLS. Seven points were marked on the trace of the crack where they were observed by the Total Station. The differences between the total station

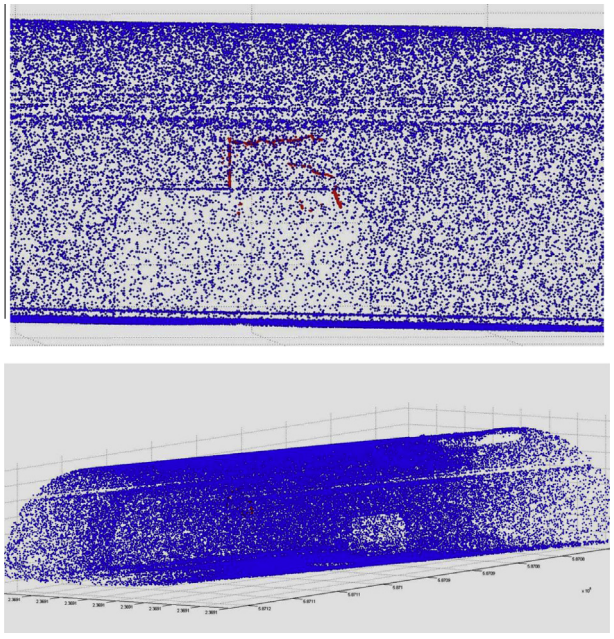

Fig. 7 Mapping the fracture in CAD format.

Table 1 The differences between the total station solution and the mapped crack by the proposed method.

X (m)	Y (m)	Z (m)	Diff. in X (mm)	Diff. in Y (mm)	Diff. in Z (mm)
169.231991	−1.032612	3.274884	38	23	19
179.418179	−0.205987	3.592571	41	11	13
168.494709	−0.668250	3.677296	35	16	15
161.843082	−0.899262	3.790217	31	12	17
154.189541	−1.160353	3.912058	19	21	14
154.793598	−1.415664	3.627939	23	14	12
152.371914	−2.172525	2.887657	27	18	10
Average			30.57143	16.42857	14.28571
Standard deviation			8.038597	4.503967	3.039424

solution and the mapped crack of the proposed method are outlined in Table 1. As it is demonstrated in Table 1, the differences between the Total Station Solution and the mapped crack by the proposed method range between 11 and 38 mm. The results give us an impression about the accuracy of the mapped cracks by the proposed method. On the other hand, the proposed method of crack mapping seems to be more accurate compared with any manual survey. It needs more updating to be more reliable in engineering applications.

5. Conclusion

By utilizing TLS in survey process, the real objects can be represented more adequately than through a single picture or collection of pictures. This is achieved by providing a higher level of details together with a good metric accuracy. The resulted models can currently be used for as-built documentation applications. In the documentation field, crack mapping represents an essential tool for as-built documentation. Automatic crack detection is highly desirable to be used to decide the appropriate rehabilitation method to fix the cracked structures and prevent any catastrophic failure.

The current paper submits a method for automatic concrete cracks detection and mapping in normally surveyed TLS data. The proposed crack detection is divided into three main parts, namely shading correction in the original images, crack detection part and mapping part. The first preprocessing part is mainly based on applying the median filter. It is concerned with image processing, by emphasizing the crack pixels, and eliminates the background values. The second detection processing part is based on Probabilistic relaxation. Moreover, for automatic detection, we applied probabilistic relaxation to prevent noise generation. Then, an improved locally adaptive thresholding was performed to detect cracks exactly. The detected crack was define in the pixel coordinate system, to map it the detected crack should be redrawn, i.e. converted from the pixel coordinate system to the TLS or global coordinate system. The results of the experiment shows an accuracy of 10–38 mm in mapping the crack compared to the results of total station survey.

References

American Society of Civil Engineers, 2000a. Guideline for Condition Assessment of the Building Envelope, ASCE Standard 30-00. ASCE, Reston, VA.

American Society of Civil Engineers, 2000b. Guideline For Structural Condition Assessment of Existing Buildings, ASCE Standard 11-99. ASCE, Reston, VA.

Amiri Parian, J., Gruen, A., 2003. A sensor model for panoramic cameras. In: Gruen and Kahmen (Ed.), 6th Conference on Optical 3D Measurement Techniques, Zurich, Switzerland, vol. 2, pp. 130–141.

Laefer, D., Gannon, J., Deely, E., 2010. Reliability of crack detection methods for baseline condition assessments. J. Infrastruct. Syst. 16 (2), 129–137.

Fujita, Y., Hamamoto, Y., 2010. A robust automatic crack detection method from noisy concrete surfaces. J. Mach. Vis. Appl.. http://dx.doi.org/10.1007/s00138-009-0244-5.

Henerson, T., 1990. Discrete Relaxation Techniques. Oxford University Press.

Leica Geosystems. Leica Scan Station C10 (2010): The All-in-One Laser Scanner for Any Application, Heerbrugg, Switzerland.

Peleg, S., 1980. A new probabilistic relaxation scheme. IEEE Transactions on Pattern Analysis and Machine Intelligence. PAMI-2 (4), 362–369.

Van Gosliga, V., R., Lindenbergh, R., Pfeifer, N., 2006. Deformation analysis of a bored tunnel by means of terrestrial laser scanning, ISPRS Technical Commission Symposium, September 2006, Dresden, Germany. International Archives of Photogrammetry, Remote Sensing and Spatial Information Systems, vol. XXXVI, Part 5: 167–172.